Hindawi
Shock and Vibration
Volume 2023, Article ID 5864013, 16 pages
https://doi.org/10.1155/2023/5864013

Research Article

A Geomechanical Model Test on the Construction Stability and Overload Failure Process of an X-Type Cross Cavern Group

Chuancheng Liu,[1,2] **Xikui Sun**,[1] **Xiufeng Zhang**,[1] **Qiangyong Zhang**,[2] **and Yang Chen**[1]

[1]*Shandong Energy Group Co., Ltd., Jinan 250101, China*
[2]*School of Civil Engineering, Shandong University, Jinan 250101, China*

Correspondence should be addressed to Chuancheng Liu; liuchuanchengsdu@163.com

Received 13 April 2023; Revised 4 June 2023; Accepted 27 June 2023; Published 25 July 2023

Academic Editor: Junyan Yi

The geological environment of the surrounding rock in deep underground engineering will become more and more complex, along with the excavation depth continuously increasing. Under these conditions of high temperatures, high seepage, high geostress, and strong excavation disturbance, the surrounding rock during underground engineering can experience obvious nonlinear deformation failure. In order to guarantee the construction, excavation, and operational safety of deep underground engineering, we have to comprehensively study the failure characteristics and deformation characteristics of the surrounding rocks of the cavern. To reveal the interaction between structures and the characteristics of overloading-induced damage and safety factor, a geomechanical model test of an X-type cross cavern group was carried out during the excavation process and overloading process. The engineering background is the URL of HLW for the geological disposal in Beishan. This is the first time that this type of geomechanical model test is being carried out. The law of displacement and stress change during the process of excavation and the law of deformation and the failure of surrounding rock in the process of overload are obtained. The test results show that the stress and displacement changes at the intersection of the caverns are most significant after excavation. The excavation's impact range is approximately 1.5 to 2 times the tunnel diameter. Under these test conditions, the safety coefficient of the crack initiation is 2.1, the safety coefficient of the local destruction is 2.5, and the safety coefficient of the general demolition is 2.9. These test results provide technical support for the design and construction of an URL for the deep buried geological disposal of HLW and have important practical significance.

1. Introduction

The relatively shallow natural resources buried on Earth are gradually disappearing due to economic development, which has led to the growing demand for resources from deep inside the Earth. Therefore, humans are constantly exploring and developing deep into the Earth to meet their demand for resources. In terms of resource and energy development, at present, the maximum mining depth of oil and gas resources has reached 7500 m [1–6]. As the excavation depth of underground caverns significantly increased, the deformation and failure characteristics of deep rock masses differ greatly from shallow rock masses, which frequently produce many unpredictable conundrums, such as zonal disintegration, large deformation, and rock bursts. So as to ensure the construction, excavation, and operation safety of deep underground laboratory, we have to comprehensively study the deformation characteristics and failure mechanisms surrounding rock during underground engineering.

Subject to the extremely harsh geological environment and complex spatial structure of deep underground engineering, traditional theoretical analysis methods often have difficulty dealing with these complex nonlinear deformation and failure problems. Numerical calculation often has difficulty simulating the process of surrounding rock mass fracture, especially the safety simulation of the whole structure is not perfect. The implementation of field tests is also limited because of their high cost. In contrast, geomechanical model tests, with their visual, intuitive, and

real-world characteristics, have become a primary method to research the failure and deformation of deep underground engineering [7]. The geomechanical model testing is the method to study specific engineering problems after reducing scale according to certain similarity principles [8]. Geomechanical models are representations of real-world physical entities. Under the condition that the similarity principle is basically satisfied, this method is able to correctly reflect the spatial relations between geology and engineering, correctly simulate the process of construction of underground engineering, and master the mechanical deformation characteristics of rock and soil media at the same time. This test can reflect the whole process of rock stress during underground engineering, from elasticity, to a plastic shape, to the final failure. This method is able to provide a foundation for the establishment of novel theoretical and mathematical models. Therefore, the geomechanical model test is able to determine the ultimate loading and failure form of the engineering and verify and supplement the numerical calculation results. Because of the above unique advantages of the geomechanical model test, this test has been widely valued and applied in geotechnical engineering both at home and abroad [9–13].

So far, significant results have been achieved in geomechanical model tests. For instance, Zhu et al. [14] and Bao et al. [15], respectively, developed different model testing systems and both innovated and improved testing techniques. Jiang et al. [16] exhibited the general demolition process of twin tunnels by a physical simulation based on the 3D printing (3DP) sandstone analogue model and presented a safety factor method for evaluating the general safety of multi-tunnel structure. Hu et al. [17] carried out the pipe-roofing method, while Shin et al. [18] validated the rationality of the umbrella arch method construction using model testing methods. Liu et al. [19] designed and developed a device to realize full section and bench method automatic excavation. Zhang et al. [20] and Zhu et al. [21] invented a multi-point displacement meter to measure the displacement changes of surrounding rock in model experiments. Wang et al. [22] applied acoustic emission to model testing to study the failure law of surrounding rock.

These applications prove the importance of the successful application of a geomechanical model test in underground engineering. Despite all these, some unresolved shortcomings of geomechanical model testing still limit its application in deep underground engineering. The previous tests were mostly planar or quasi-three-dimensional, which cannot reflect the actual state of the ground stress. Furthermore, most of the previous tests simulated a single chamber, not a complex chamber group. Moreover, most of the excavation methods in the test use manual drilling with low accuracy.

In this paper, a geomechanical model test on an X-type cavern group composed of two intersecting horizontal tunnels with three-core arches was carried out, using the URL for the deep buried geological disposal of HLW in the Beishan area, China, as a prototype. We evaluate the overall stability and inter-chamber interaction of the cavern group during construction and excavation. In addition, we use an overload test to estimate the overloading damage characteristics and overall safety factors of the whole system. We then prove the validity of the designed plan and offer technical support for the design and construction of the URL for the deep buried geological disposal of HLW.

2. Geomechanical Model Test of the Excavation Process

2.1. Project Overview. Nuclear waste, or radioactive waste, can be divided into low-level radioactive waste, medium-level radioactive waste, and high-level radioactive waste (HLW) based on radioactivity level. At present, there are many mature technologies for the final secure disposal of low-level and medium-level radioactive waste. However, the safe disposal of HLW is a worldwide problem because it contains highly toxic radionuclides with long half-lives. After decades of research and practice, the currently accepted viable option to securely dispose HLW is deep geological disposal. Using this method, high-level radioactive waste is buried deeply in a geological body about 1000 meters from the surface of the Earth, thereby permanently isolating it from the human living environment [23, 24]. Underground projects for the burial of HLW are known as geological repositories. Since the waste in a geological repository is highly toxic and has a long half-life, it is required that the life of the geological repository should be at least 1×104 a. This requirement is not present in any other project. Furthermore, the entire disposal process is unprecedented. Existing projects are unable to provide suitable engineering experience. Therefore, most countries believe that the underground laboratories must be built first before the whole project can be implemented, providing necessary technical support and practical experience through on-site experiments and research. This research facility is known as the URL for the disposal of HLW.

MoEP (the Ministry of Environment Protection) and CAEA (China Atomic Energy Authority) ultimately selected the Xinchang site as the first geological disposal site for deep burial of HLW in China [25, 26], which is located in the middle of the Beishan area in Gansu Province, about 135 kilometers from Jiayuguan City (see Figure 1).

The terrain of this area is mainly characterized by scattered low hills, whose average altitude is approximately 1700 m. The terrain fluctuation does not change much, generally not exceeding 30 m. More specifically, the Beishan URL is built within a block of granite body of the Xinchang site, which is 22 kilometers long and 7 kilometers wide. The main rock types in this area are granodiorite and monzogranite. The bedrock structure is complete and the groundwater is poor. The initial stress function of the proposed field is as follows:

$$\left.\begin{aligned} \sigma_H &= 0.0305H \text{ (MPa)}, \\ \sigma_h &= 0.0208H \text{ (MPa)}, \\ \sigma_v &= 0.0268H \text{ (MPa)} \end{aligned}\right\}, \tag{1}$$

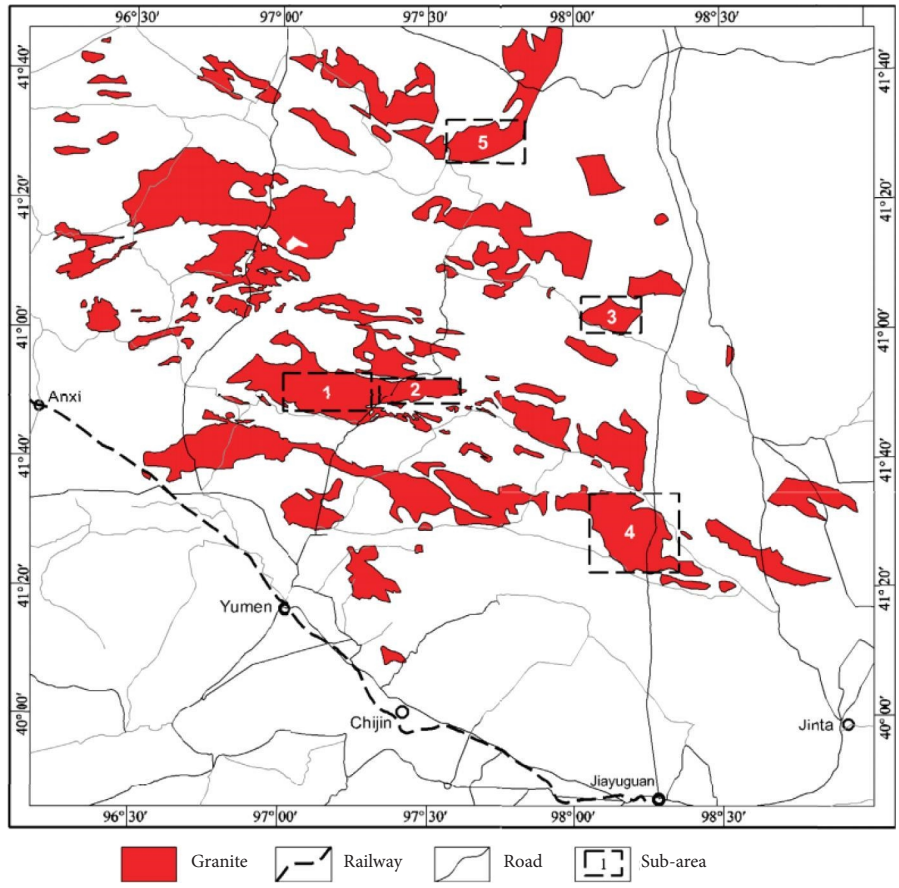

1 – Jiujing sub-area; 2 – Xinchang sub-area; 3 – Yemaquan sub-area; 4 – Shazaoyuan sub-area; 5 – Suanjingzi sub-area

Figure 1: Geographical location of the Beishan area (from [25]).

where H is the buried depth of the chamber (m) and σ_H, σ_h, and σ_V represent the maximum and minimum horizontal principal stresses and vertical stresses, respectively.

In the preliminary design of the Beishan underground laboratory (see Figure 2(a)), the overall structure of the laboratory included a transportation ramp, three potholes (two for ventilation and one for personnel lift), and two horizontal test areas for in situ experiments. The buried depth of the main horizontal test area is −560 m, while the auxiliary horizontal test area is −240 m. In the design process, considering the convenience of transportation, the junction between the transportation ramp and the main roadway was designed as an X-type intersection (see Figure 2(b)). To study the reliability of the modified design scheme, the interactions between X-type cross chambers, and the overload safety factor, we selected a main roadway with a depth of −560 m and the drift with a depth of −560 m as the research objects. The area is 125 m × 125 m × 100 m (length × height × width), including a three-core arched main roadway (cross section size of 8 × 7.67 m) and a three-core arched drift (cross section size of 8 × 7.67 m).

2.2. Model Test System. In order to investigate whether the initial geostress state of the model body matches the actual state of the prototype accurately, we developed a true triaxial ultra-high-pressure loading system (see Figure 3).

The main technical advantages of the test system are as follows. ① The maximum load is 45,000 kN, whose loading accuracy is 1.5% F.S. ② The external dimension of the reaction force device is 5.05 × 4.85 × 3.6 m, and the model body size is 2.5 × 2.5 × 2 m. ③ It realizes the visualization, intelligentization, and digitization of the displacement measurements and loading/unloading.

2.3. Similar Conditions. Once similar conditions are satisfied, the geomechanical model test can truly simulate the entire construction process [8]. Based on the laws of similarity, the following relationships should also be satisfied [27–29]:

$$\begin{aligned} C_\sigma &= C_\gamma C_L, \\ C_\delta &= C_\varepsilon C_L, \\ C_\sigma &= C_\varepsilon C_E, \\ C_\varepsilon &= C_f = C_\varphi = C_\mu = 1, \end{aligned} \tag{2}$$

where C represents the similarity coefficient of different physical quantities and subscripts represent different physical quantities, respectively.

We selected C_L to be 50 based on the range of the project and the scale of the test system. The total size of the model body is 2500 mm × 2500 mm × 2000 mm (length × height × width)

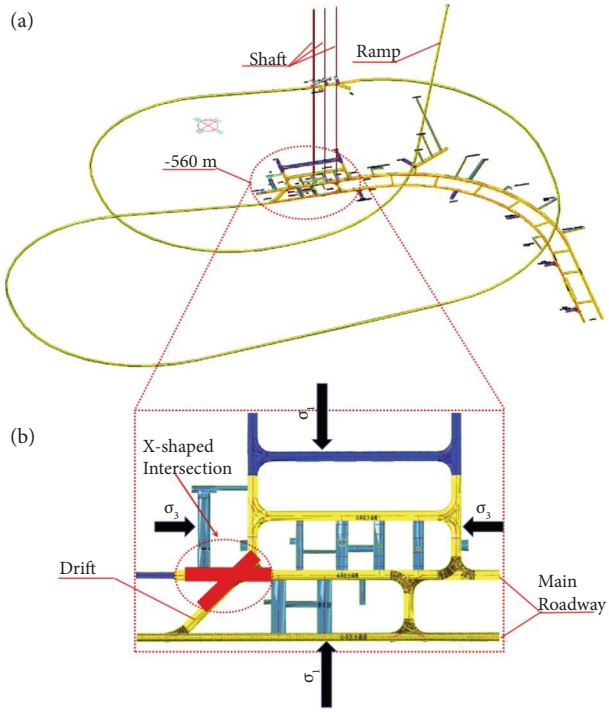

Figure 2: Preliminary design scheme of underground laboratory structure (modified from [25]).

Figure 3: Three-dimensional geomechanical model test system: (1) reaction force device; (2) ground stress simulation system; (3) displacement monitoring system; (4) reaction force device; (5) micro-TBM excavation device.

accordingly, which consists of the main roadway and the drift (see Figure 4).

2.4. Analogue Material. The mechanical and physical parameters of the original rocks measured by the experiments are shown in Table 1. According to the similarity principle [8], we have determined $C_L = 50$ and $C_\gamma = 1$, so the theoretical values of the similar materials can be calculated (see Table 1).

Many scholars [30–32] have researched massive analogue materials of the model tests. These researchers have developed a variety of analogue materials with different properties by using different raw materials for matching. Each material has its own advantages and disadvantages. In this study, the analogue material we used has obtained a Chinese invention patent [33]. Based on the theoretical value of the analogue material in Table 1, we conducted a uniaxial compression test, a Brazilian splitting test, a direct shear test, and a triaxial compression test by adjusting the proportions of the components of IBSCM. An orthogonal test was carried out to obtain a mixed proportion of analogue materials (see Table 2), and the measured values of the mechanical parameters satisfy similar conditions (see Table 1).

2.5. Test Model Construction. The test model was constructed by the layered compaction and air drying process, which has been patented in China [34]. The basic process is as follows (see Figure 5): ① according to the mix proportion obtained in Table 2, weigh each component and configure the alcohol rosin solution; ② pour the weighed aggregate (iron powder, quartz sand, and barite powder) into the blender and stir well; ③ add the alcohol rosin solution and mix well after the aggregate is stirred evenly; ④ pour the mixed material into the reaction force device and spread the material in layers from the bottom to the top; ⑤ compact each layer of material at a fixed pressure via the loading system of the test system and then dry it with a high-powered fan; ⑥ install the measurement elements around the cavern according to the design elevation; and ⑦ repeat steps ①~⑥ until the model is complete.

Figure 6 shows the positions of the monitoring sensors. All monitoring sensors are installed at the key parts in six monitoring sections.

2.6. Excavation Method. After the model was complete, the nonuniform distribution diagram of the initial in situ stress gradient of the model was calculated from equation (1) and similar conditions (see Figure 7).

We then carried out true 3D loading on the model boundary using the experimental system until the requirements of Figure 7 were met. After the loading was completed, the boundary load was kept constant, and the pressure was stabilized for 24 hours. We kept the pressure constant and excavated the cavern group according to the actual excavation steps. The control parameters of the cavern group's excavation are as follows.

Both the main roadway and drift were excavated by our self-developed micro-TBM excavation device (see Figure 8). Firstly, the excavation device was located and fixed on the reaction force device of the test system with the assistance of the total station. Then, the caverns were precisely excavated according to the sequence of the main roadway first and the drift second. After each excavation step was completed, we waited for 10–15 minutes, and the data were recorded in real time. Then, the next excavation was conducted until all caverns were excavated.

2.7. Test Result. After the excavation was completed, the intersecting position of the cavern was accurate, the wall was smooth, and the size of the excavation chamber was consistent with the design scheme (see Figure 9).

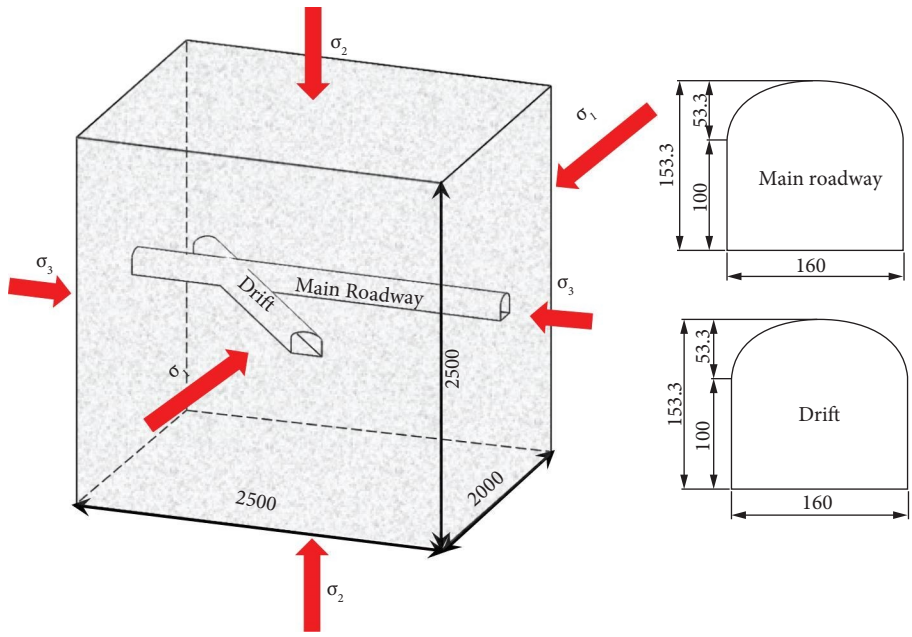

Figure 4: Structure and size of the test model (all length units in the figure are mm).

We convert all the measured data to the values of the prototype according to the similarity criteria for easy analysis and understanding.

The displacement changes linearly with the excavation process. It is obvious that when the excavation face reaches a certain monitoring section, the displacement of this section changes suddenly. The excavation face continues to advance, and the displacement gradually tends to be stable (see Figure 10).

During the excavation process, there is an obvious law of meeting influence between adjacent chambers. The excavation of the drift will lead to the sudden change of the rock displacement around the main roadway. Accordingly, the excavation of the main roadway will also lead to the sudden change of the rock displacement around the drift.

The closer the surrounding rock around the chamber is to the chamber wall, the greater the displacement change is, which is basically called the law of linear growth. The displacement of surrounding rock at nonintersection is less than that at intersection, and the reduction range is about 30%. The maximum displacement in the model appears at the vault position at the intersection of two chambers. Through the observation of displacement changes, it can be found that the influence range of excavation disturbance at the waist of the chamber is about 1.5 times the chamber span, while the influence range of excavation at the vault can reach about 2.0 times the chamber height (see Figure 11).

The farther the surrounding rock around the chamber is from the chamber wall, the smaller the value of radial stress release is, and correspondingly, the smaller the value of tangential stress increase is. No tensile stress was detected in the surrounding rock of the model, and the surrounding rock of the cave was in a state of compression. Also, the maximum stress detected is only 38.89 MPa, which is far less than the compressive strength of rock, and all surrounding rocks are in a stable state. It is found that the influence range of the excavation disturbance of the chamber is about twice the span of the chamber (see Figure 12).

3. Geomechanical Model Test of the Overloading Process

To further assess the overall safety factors of the URL, we carried out overloading tests on the model after excavation. The methods of the overloading model test are as follows.

① After the model test of the excavation process is completed, the gravity stress and tectonic stress are increased step by step, and the increase of each step is 0.1 times that of the initial ground stress. ② After the overloading of each step is applied, the pressure is stabilized for at least half an hour. The test data are recorded after stabilization. Meanwhile, the failure process of surrounding rock is noticed synchronously by the HD camera placed in the cavern. ③ The overloading process is carried out step by step until the chamber group noticeably collapses.

Four HD cameras were installed in the excavated caverns, the specific positions of which are shown in Figure 13.

3.1. Destruction Phenomena and Fracturing Patterns. Under 1.1–1.7 times overloading, all the interior parts of the cave, including the junction, remain intact, and the surrounding rock does not show any cracks or cracking damage, indicating that the cavern group as a whole remains in a stable state under an overloaded state of 1.1~1.7 times (see Figure 14).

As the overloading continues to increase, when it reaches 1.8 times, visible micro-cracks begin to appear at the intersection of the caverns (see Figure 15). For instance, micro-cracks occur at the waist of the cavern

Table 1: Mechanical and physical parameters.

Category	Unit weight (kN/m^3)	Deformation modulus (GPa)	Uniaxial compressive strength (MPa)	Tensile strength (MPa)	Cohesion (MPa)	Friction angle (°)	Poisson's ratio
Original rock	26.80	49.17	132.37	6.86	28.13	50.6	0.264
Theoretical value of analogue material	26.80	0.983	2.647	0.134	0.563	50.6	0.264
Measured value of analogue material	26.2–27.1	0.955–0.992	2.611–2.683	0.123–0.142	0.541–0.571	49.9–50.6	0.25–0.27

Table 2: The proportion of each material.

Component	Rosin	Alcohol	Quartz sand	Barite powder	Iron powder
Ratio to the total weight of materials (%)	4.9	1.1	13.8	24.9	55.3

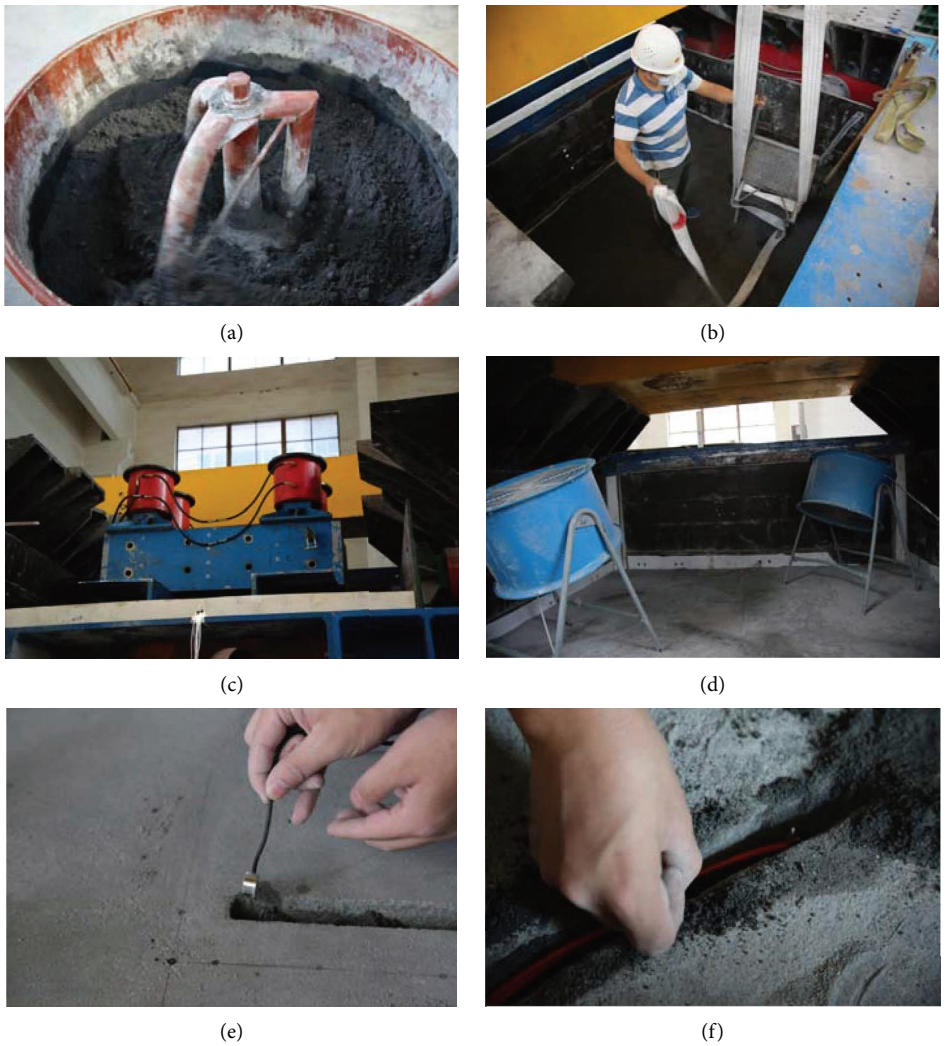

Figure 5: Model construction process: (a) mix material; (b) pour in the reaction force device; (c) compact materials; (d) air-dry with large fans; (e) install pressure cell; (f) install displacement measurement point.

intersection. When the overloading multiple continues to increase to 2.1, obvious cracks appear in some positions. For instance, cracks appear at the vault of the cavern at the intersection.

Under the action of 2.2–2.5 times overload, the microcracks in the cavern began to expand gradually. With a continuous increase of the loading, the cracks in the interior of the cavern gradually become wider and longer, which leads to compression shear failure or tension shear failure in the surrounding rock (see Figure 16). The specific performance is as follows. Continuous spalling and roof collapses occur at the intersection; the cracks in the main roadway vault gradually expand, forming a longitudinal crack with a width of about 1–2 mm, and roof collapse occurs.

Under the action of 2.6–2.9 times overload, obvious damage began to appear in all parts of the cavern group (see Figure 17). We can observe that the cracks in the rock of the vault at the junction are continuously expanding and penetrating, so roof collapse and spalling of large blocks occur, and the side walls on both sides are obviously contracted and deformed inward. The cracks in the main roadway vault then continue to expand, and serious roof collapses occur. The destruction of the acute part of the intersection is more serious than that of the obtuse part.

3.2. Overloading-Induced Deformation. Under the action of 1.1–1.7 times overload, all the displacement of the cavern group measured increases compared with that before the

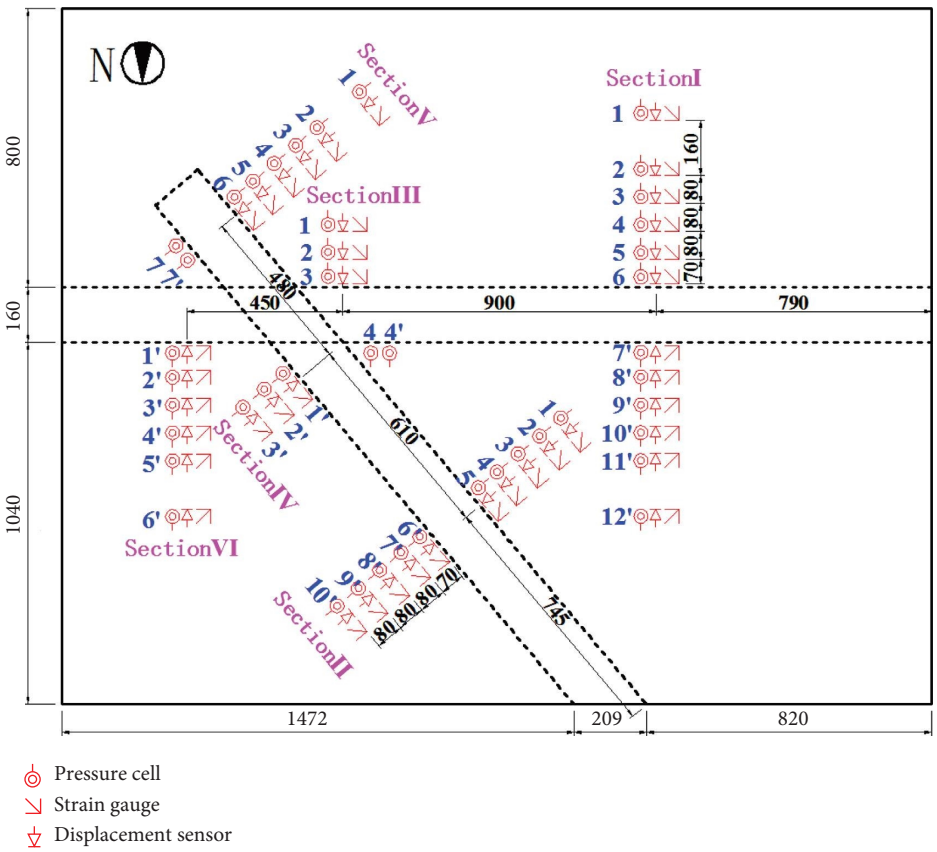

Figure 6: Design drawing of the monitoring sensor positions.

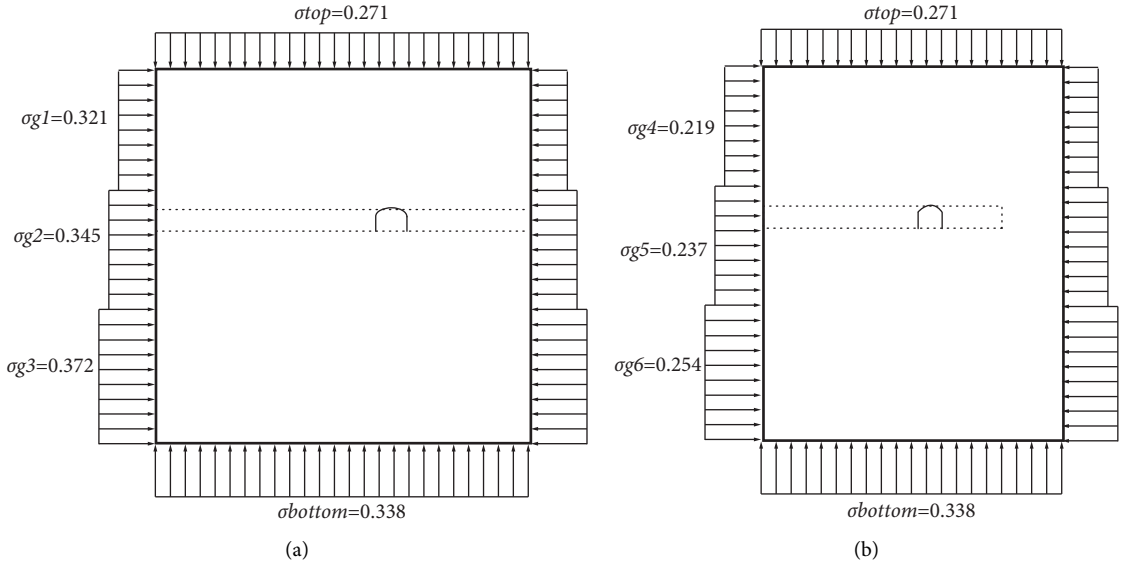

Figure 7: Initial in situ stress distribution of the model. (a) Orientation of major principal stress. (b) Orientation of minor principal stress (the unit of stress is MPa).

overload, but the overall trend of the displacement change curve remains stable, and the change value of displacement still does not exceed millimeter magnitude (see Figure 18). The max change value of displacement still occurs at the point nearest to the cavern wall (see curve 1.7P in Figure 19). Among them, the displacement of the vault at the intersection is the largest, which is about 6 mm. From the displacement curve and the video observation in the cavern, it can be seen that the chamber group still remains stable at 1.1–1.7 times overload.

Figure 8: Photos of the micro-TBM excavation device.

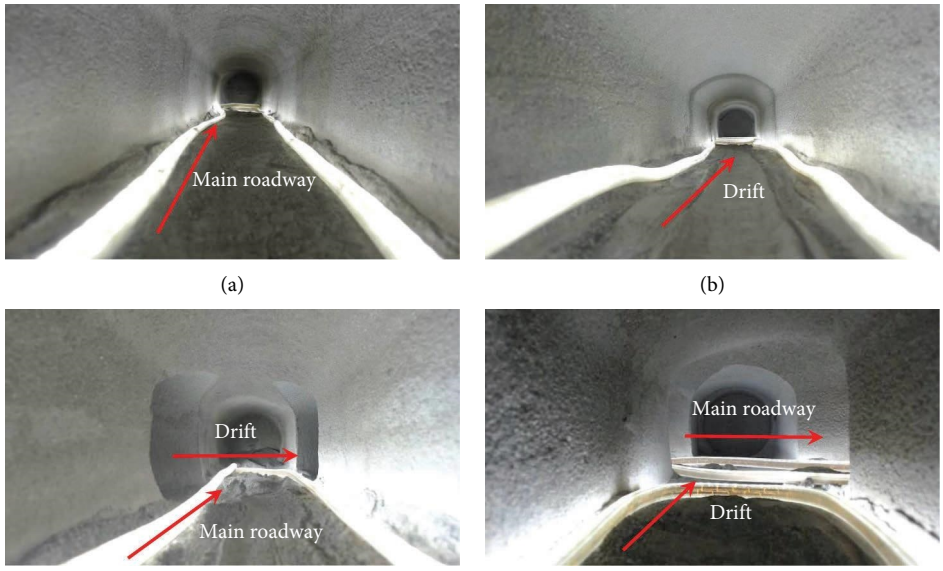

Figure 9: Pictures of the chamber group after excavation: (a) main roadway; (b) drift; (c) the intersection of the main roadway and drift; (d) the intersection of the drift and main roadway.

Under 1.8–2.1 times overload, the displacement variation continues to increase, and the further it is to the wall, the smaller the displacement increment is (see curve 2.1P in Figure 19). The displacement of the vault at the intersection is the largest, which is about 59 mm. In general, the slope of the overall displacement curve of the cavern group began to increase gradually at this stage. Combined with the video observation results, under 1.8–2.1 times overload, the cavern group still remains basically stable, except for local cracks and slag falling.

Under 2.1–2.5 times overload, the curve of the displacement overload increases sharply, both the change rate and the absolute value of displacement increase significantly, and there is a sudden change phenomenon (see curve 2.5P in Figure 19). For instance, the maximum displacement increment of the vault at the intersection reaches 83.25 mm. Comparing image data, we can observe that under 2.5 times overload, the cavern group enters the stage of local damage.

Under 2.6–2.9 times overload, the change slope of the displacement of all parts around the cavern increases rapidly (see curve 2.9P in Figure 19), and with a large-scale sudden change, the displacement of all parts around the cavern cannot remain stable and increases rapidly; in the vault section, where the main roadway and the drift cross, the maximum displacement increment reaches 123.25 mm. Combined with the video observation, it can be seen that

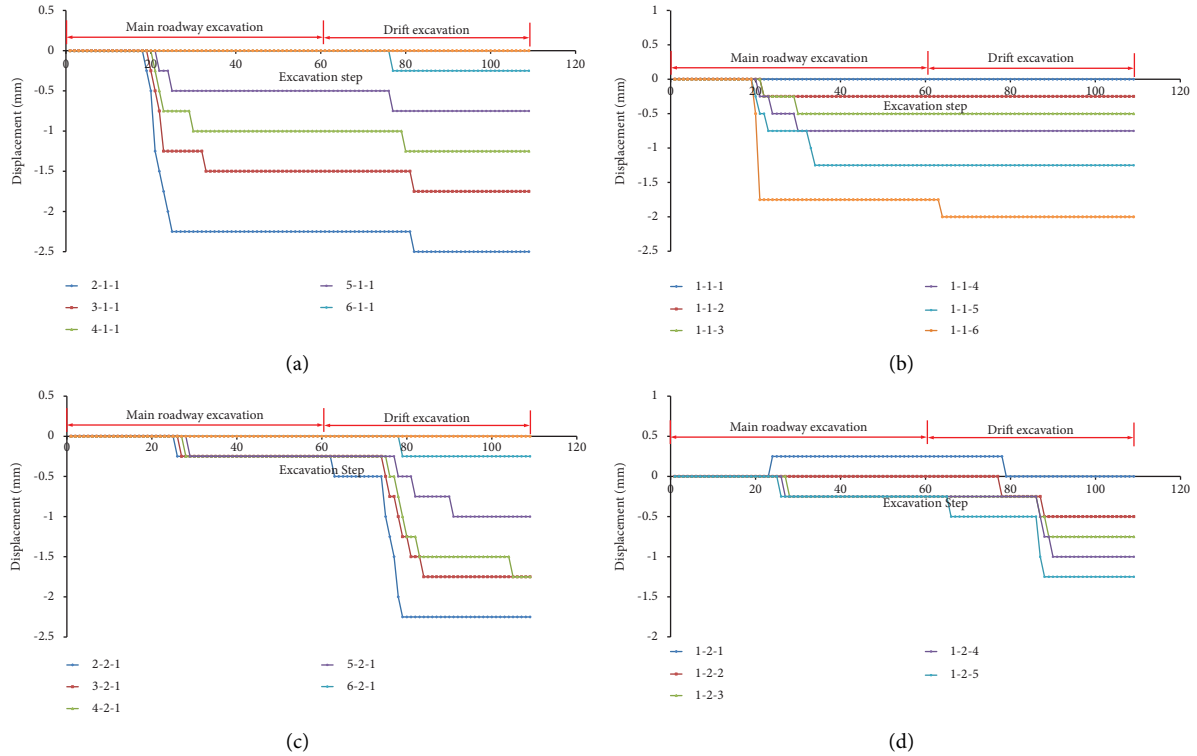

Figure 10: The time history of displacements during the excavation: (a) main roadway in section I; (b) main roadway in section I; (c) drift in section II; (d) drift in section II.

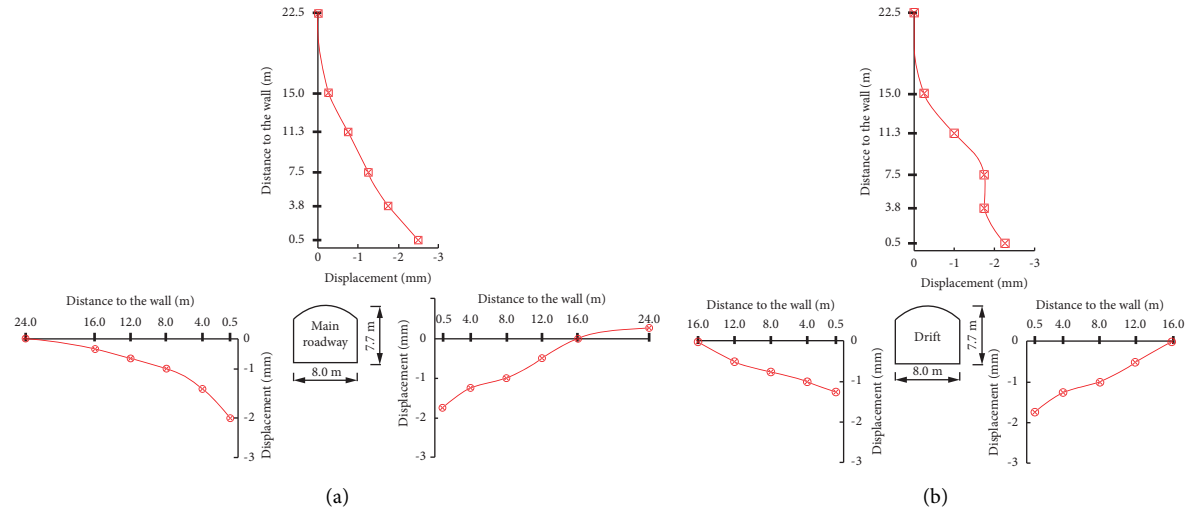

Figure 11: Variation of the displacement of chambers: (a) main roadway in section I; (b) drift in section II.

under 2.9 times overload, the chamber group enters the stage of general demolition.

In summary, there is a nonlinear growth relationship between the overloading and the monitored deformation of tunnel. For example, when the overloading is small, the rate of deformation change is small, and as the overloading increases, the rate of deformation change gradually increases until a sudden change occurs, causing damage to the tunnel.

4. Discussion

In this study, we found that the influence range of excavation is about 1.5–2.0 times the diameter of the cavern. This range is basically consistent with the results of other engineering cases [35, 36]. At the same time, other scholars conducted some field tests in Beishan area, and the test results indicated that the excavation disturbed zone is about 1.5 times the cavern's span [37–42].

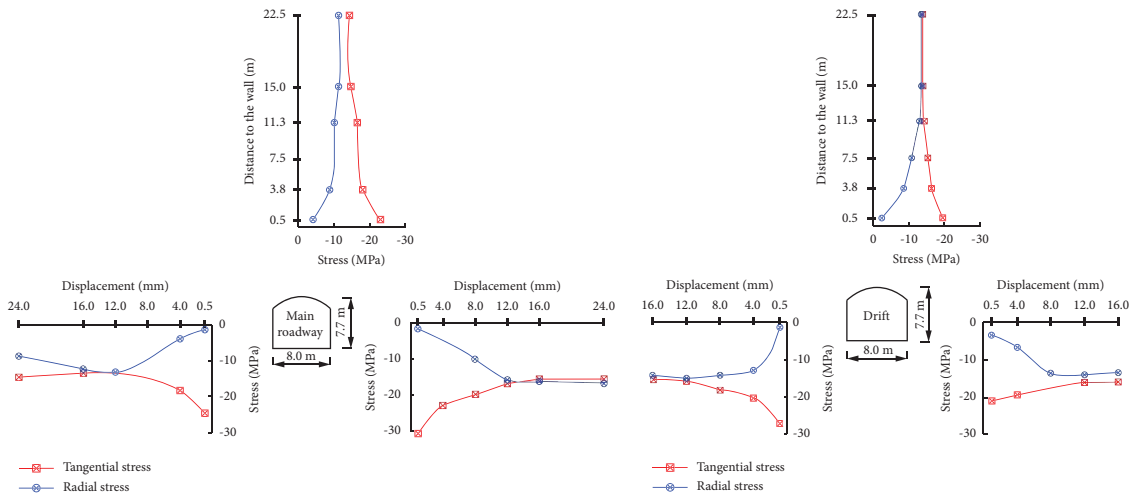

Figure 12: Variation of the stress of chambers: (a) main roadway in section I; (b) drift in section II.

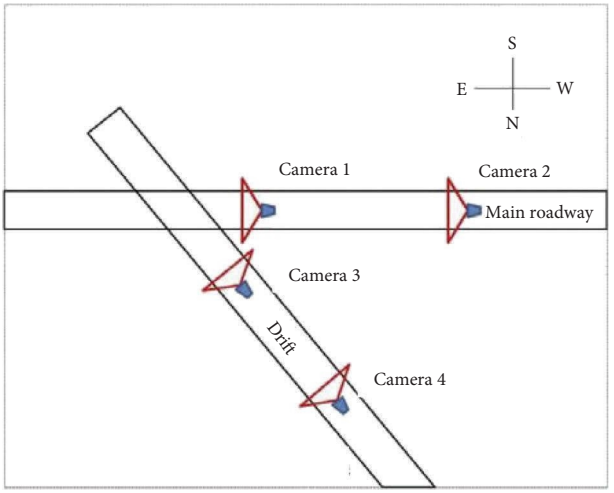

Figure 13: Layout of HD camera.

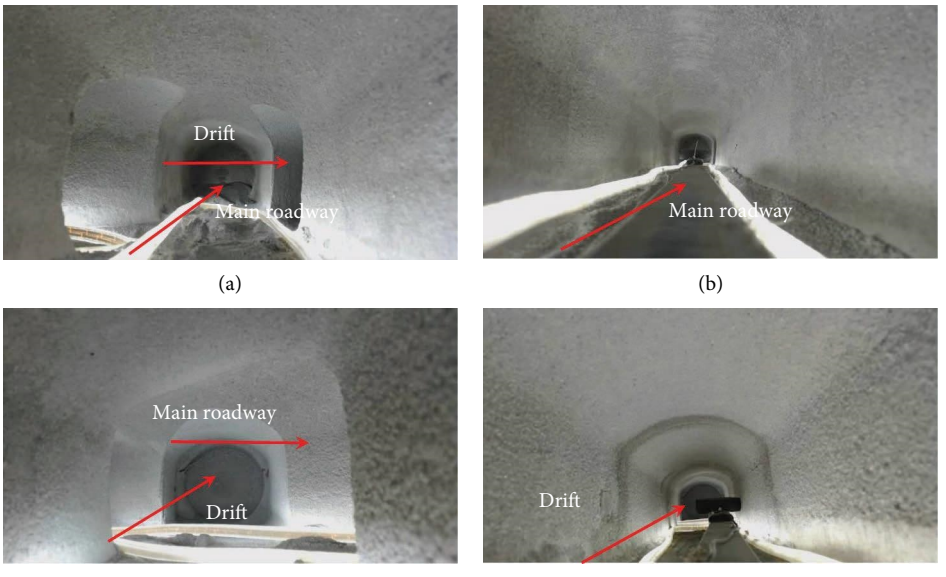

Figure 14: Photos of the caverns under the overloading of 1.7P: (a) from camera 1; (b) from camera 2; (c) from camera 3; (d) from camera 4.

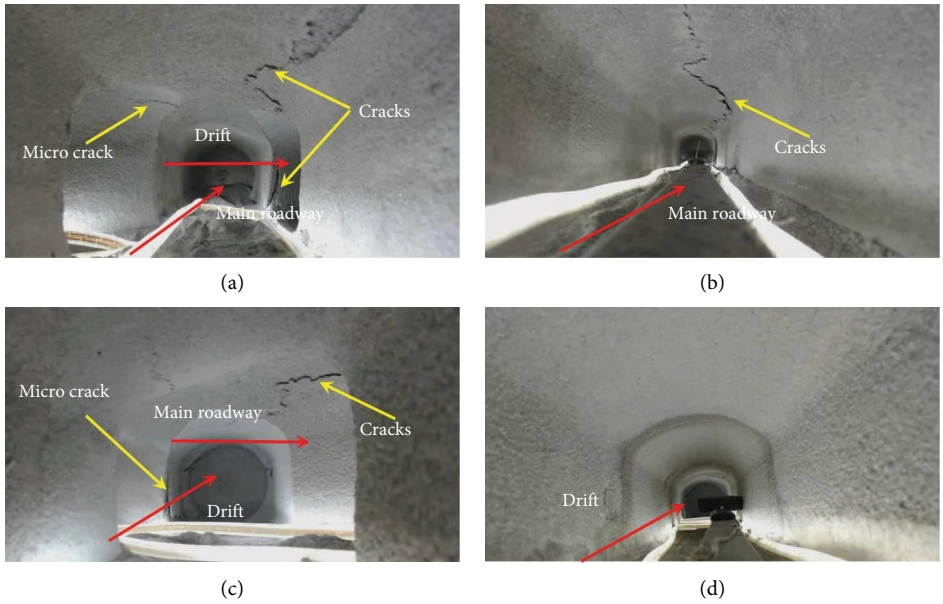

Figure 15: Photos of the caverns under the overloading of 2.1P: (a) from camera 1; (b) from camera 2; (c) from camera 3; (d) from camera 4.

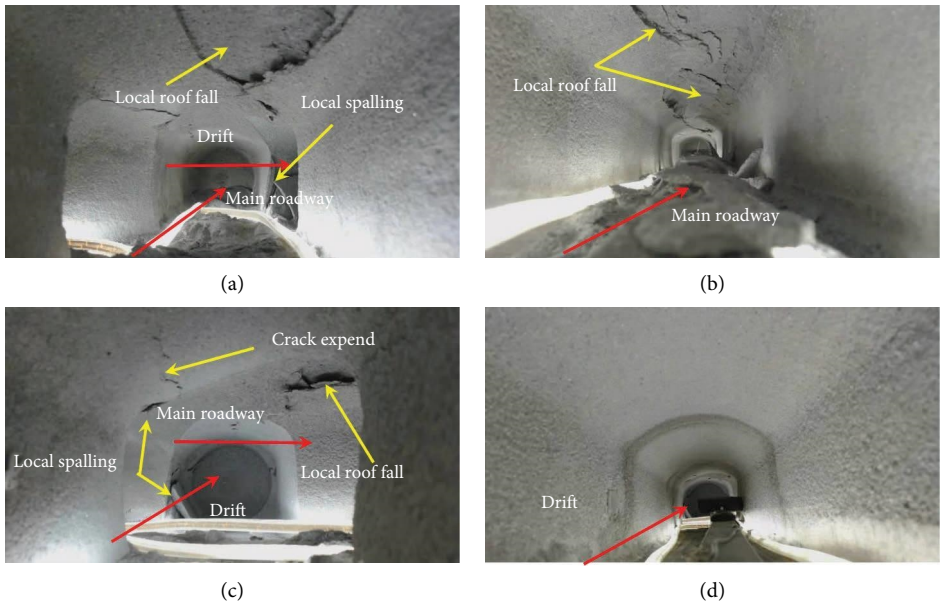

Figure 16: Photos of the caverns under the overloading of 2.5P: (a) from camera 1; (b) from camera 2; (c) from camera 3; (d) from camera 4.

We found the overloading safety factor of X-type cross chamber group. Under 1.1–1.7 times overload, there were no visible cracks in any parts of the chamber group, and the chamber group remained stable. Under 1.8–2.1 times overload, there were micro-cracks visible at the intersection of the caverns; the displacement of the surrounding rock increased gradually at first (remaining minimal), and the chamber group still remained stable. Under 2.5 times overload, the displacement began to increase sharply, both the change rate and the absolute value of displacement increase significantly, there is a sudden change phenomenon, and the chamber group entered local destruction. Under 2.9 times overload, the displacement of all parts around the tunnel could not remain stable and increased rapidly. The chamber group entered the stage of general demolition. It can be determined that under these experimental conditions, the safety coefficient of crack initiation is 2.1; the safety coefficient of local destruction is 2.5; and the safety coefficient of general demolition is 2.9.

However, in fact, there are still some differences between the overload safety factor and the actual safety factor, which is also one of our follow-up research contents. We will

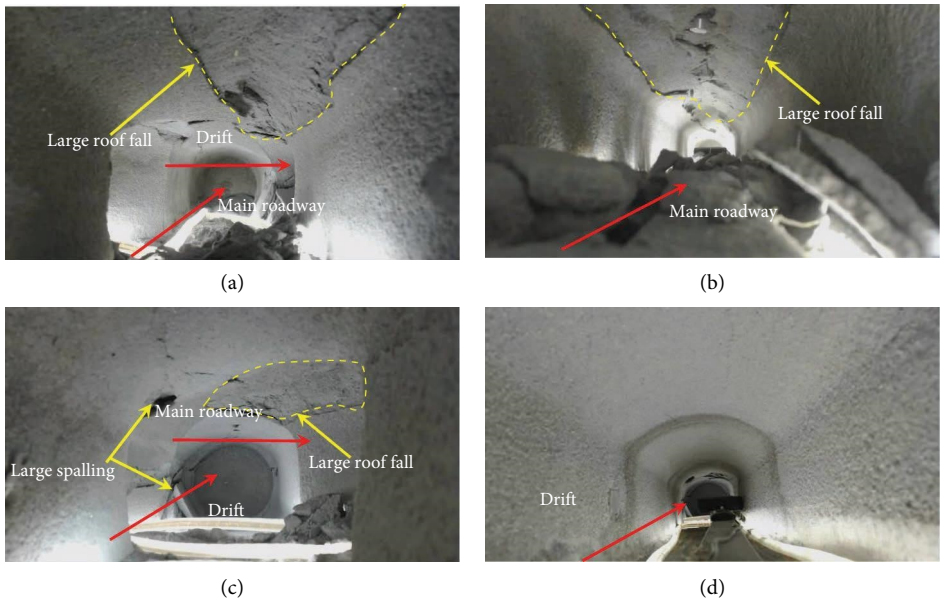

Figure 17: Photos of the caverns under the overloading of 2.9P: (a) from camera 1; (b) from camera 2; (c) from camera 3; (d) from camera 4.

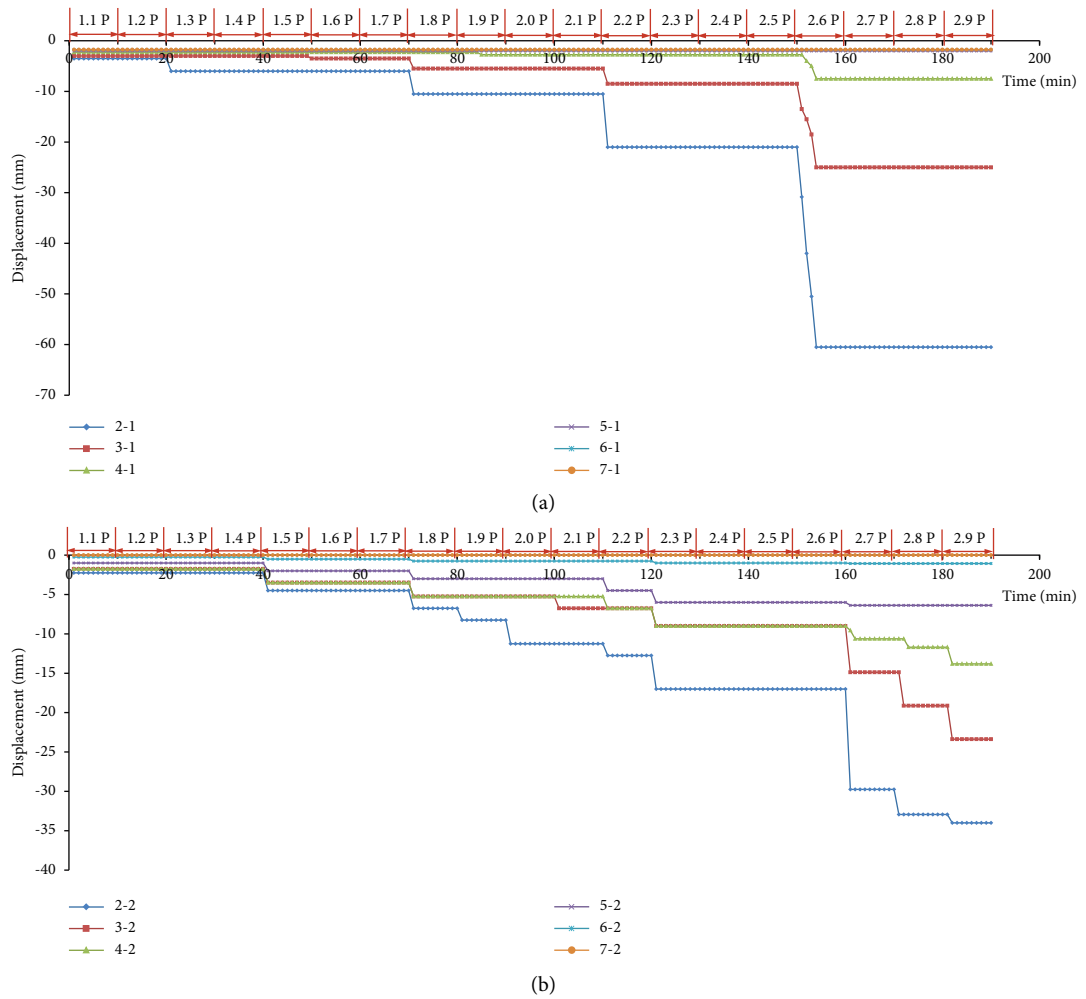

Figure 18: Continued.

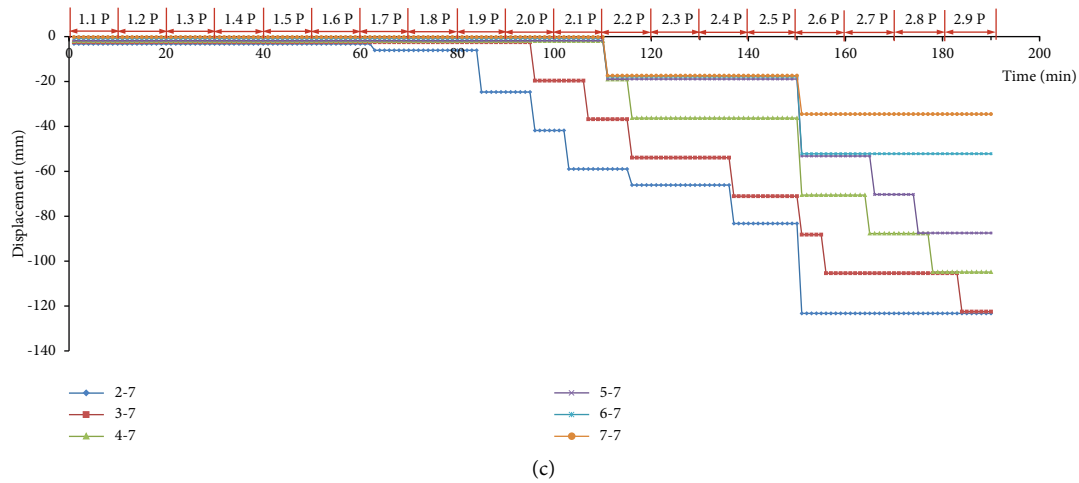

FIGURE 18: The time history of displacements of overload time: (a) main roadway in section I; (b) drift in section II; (c) the intersection vault in section VII.

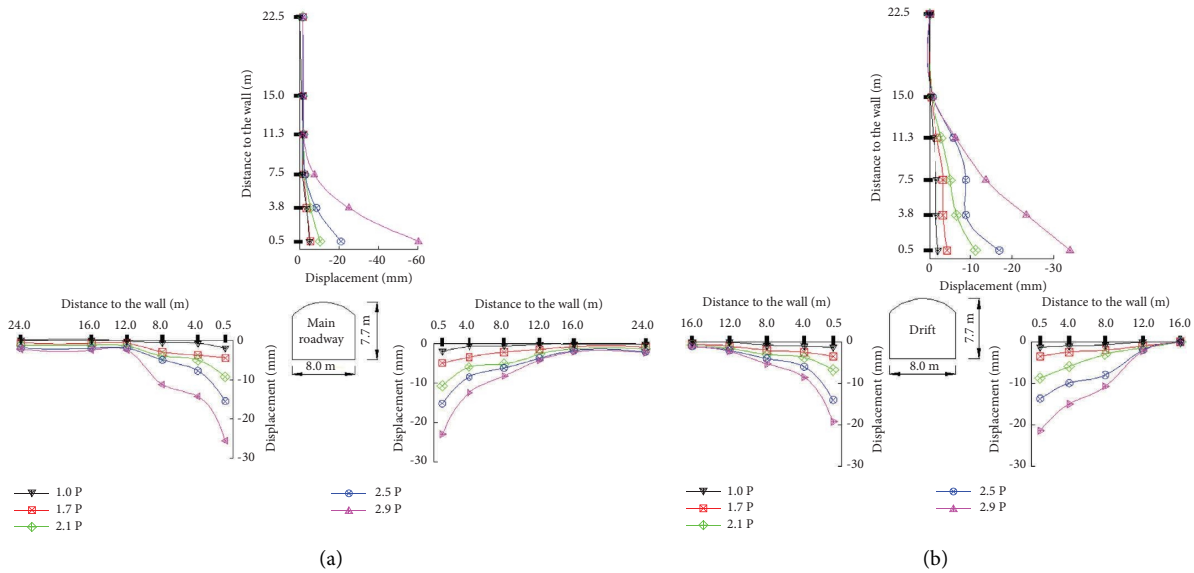

FIGURE 19: The spatial variation in the displacements in the stage of overloading: (a) main roadway in section I; (b) drift in section II.

further discuss the safety factor of caverns through numerical simulation methods such as the strength reduction method.

5. Conclusion

We carried out a geomechanical model test on an X-type cavern group composed of two intersecting horizontal tunnels with three-core arches. Our conclusions are as follows:

(1) After excavation, the closer the surrounding rock around the chamber is to the chamber wall, the greater the displacement change is, which is basically called the law of linear growth. The maximum displacement in the model appears at the vault position at the intersection of two chambers.

(2) Under these experimental conditions, the safety coefficient of initiation is 2.1, the safety coefficient of local destruction is 2.5, and the safety coefficient of general demolition is 2.9.

(3) The destruction of the acute part of the intersection is more serious than that of the obtuse part. The design scheme should be further optimized, and the X-type intersection should be changed into the scheme of vertical intersection.

(4) So as to ensure the safety of project and operation, it is suggested to focus on monitoring the intersection and to consider whether to add support according to the monitoring results.

These test results provide technical support for the design and building of an URL for the deep buried geological

disposal of HLW and thus have important practical significance.

Data Availability

The data used to support the findings of this study are available from the corresponding author upon request.

Conflicts of Interest

The authors declare that there are no conflicts of interest regarding the publication of this paper.

Acknowledgments

This research was funded by the Shandong Province Postdoctoral Innovation Project (SDCX-ZG-202203055), Preliminary Research Project of the Underground Laboratory for the Geological Disposal of High-Level Radioactive Waste of China (no. YK-KY-J-2015-25), National Key Research and Development Project (2020YFB1314200), and Major Scientific and Technological Innovation Project in Shandong Province (no. 2019SDZY02).

References

[1] H. P. Xie, F. Gao, and Y. Ju, "Research and development of rock mechanics in deep ground engineering," *Chinese Journal of Rock Mechanics and Engineering*, vol. 34, pp. 2161–2178, 2015.

[2] J. Q. Deng, Q. Yang, Y. R. Liu, and Y. W. Pan, "Stability evaluation and failure analysis of rock salt gas storage caverns based on deformation reinforcement theory," *Computers and Geotechnics*, vol. 68, pp. 147–160, 2015.

[3] V. N. Reva, "Stability criteria of underground workings under zonal disintegration of rocks," *Journal of Mining Science*, vol. 38, no. 1, pp. 31–34, 2002.

[4] E. J. Sellers and P. Klerck, "Modelling of the effect of discontinuities on the extent of the fracture zone surrounding deep tunnels," *Tunnelling and Underground Space Technology*, vol. 15, no. 4, pp. 463–469, 2000.

[5] M. A. Guzev and A. A. Paroshin, "Non–euclidean model of the zonal disintegration of rocks around an underground working," *Journal of Applied Mechanics and Technical Physics*, vol. 42, no. 1, pp. 131–139, 2001.

[6] K. Duan, Y. Ji, W. Wu, and C. Y. Kwok, "Unloading-induced failure of brittle rock and implications for excavation-induced strain burst," *Tunnelling and Underground Space Technology*, vol. 84, pp. 495–506, 2019.

[7] M. A. Meguid, O. Saada, M. A. Nunes, and J. Mattar, "Physical modeling of tunnels in soft ground: a review," *Tunnelling and Underground Space Technology*, vol. 23, no. 2, pp. 185–198, 2008.

[8] E. Fumagalli, *Statical and Geomechanical Models*, Springer Press, New York, NY, USA, 1973.

[9] S. Tai, "Development of geomechanic model experiment techniques," *Journal of Yangtze River Scientific Research Institute*, vol. 18, pp. 32–36, 2001.

[10] W. Y. Zhou, R. Q. Yang, Y. R. Liu, and P. Lin, "Research on geomechanical model of rupture tests of arch dams for their stability," *Journal of Hydroelectric Engineering*, vol. 24, pp. 50–57, 2005.

[11] A. M. Chen, J. C. Gu, J. Shen, A. Q. Ming, and L. Y. Gu, "Application study on the geomechanical model experiment techniques," *Chinese Journal of Rock Mechanics and Engineering*, vol. 23, p. 3785, 2004.

[12] P. H. S. W. Kulatilake, W. He, J. Um, and H. Wang, "A physical model study of jointed rock mass strength under uniaxial compressive loading," *International Journal of Rock Mechanics and Mining Sciences*, vol. 34, no. 3-4, pp. 165.e1–165.e15, 1997.

[13] K. Bakhtar, "Impact of joints and discontinuities on the blast-response of responding tunnels studied under physical modeling at 1-g," *International Journal of Rock Mechanics and Mining Sciences*, vol. 34, no. 3-4, pp. 21.e1–21.e15, 1997.

[14] W. S. Zhu, Q. B. Zhang, Y. Li, L. F. Sun, L. Zhang, and W. H. Zheng, "Development of large-scale physical model test system under true triaxial loading and its applications," *Chinese Journal of Rock Mechanics and Engineering*, vol. 29, pp. 1–7, 2010.

[15] Z. Bao, Y. Yuan, and H. T. Yu, "Multi-scale physical model of shield tunnels applied in shaking table test," *Soil Dynamics and Earthquake Engineering*, vol. 100, pp. 465–479, 2017.

[16] Q. Jiang, X. P. Liu, F. Yan, Y. Yang, D. Xu, and G. Feng, "Failure performance of 3DP physical twin-tunnel model and corresponding safety factor evaluation," *Rock Mechanics and Rock Engineering*, vol. 54, pp. 109–128, 2020.

[17] X. Hu, T. Fang, J. Chen, H. Ren, and W. Guo, "A large-scale physical model test on frozen status in freeze-sealing pipe roof method for tunnel construction," *Tunnelling and Underground Space Technology*, vol. 72, pp. 55–63, 2018.

[18] J. H. Shin, Y. K. Choi, O. Y. Kwon, and S. D. Lee, "Model testing for pipe-reinforced tunnel heading in a granular soil," *Tunnelling and Underground Space Technology*, vol. 23, no. 3, pp. 241–250, 2008.

[19] C. C. Liu, Q. Y. Zhang, and W. Xiang, "Development and application of micro automatic excavation device for model test of underground engineering," *Geotechnical and Geological Engineering*, vol. 38, no. 5, pp. 4847–4862, 2020.

[20] Q. B. Zhang, L. He, and W. S. Zhu, "Displacement measurement techniques and numerical verification in 3D geomechanical model tests of an underground cavern group," *Tunnelling and Underground Space Technology*, vol. 56, pp. 54–64, 2016.

[21] W. S. Zhu, Y. Li, S. C. Li, S. G. Wang, and Q. B. Zhang, "Quasi-three-dimensional physical model tests on a cavern complex under high in-situ stresses," *International Journal of Rock Mechanics and Mining Sciences*, vol. 48, no. 2, pp. 199–209, 2011.

[22] S. G. Wang, Y. R. Liu, Z. F. Tao et al., "Geomechanical model test for failure and stability analysis of high arch dam based on acoustic emission technique," *International Journal of Rock Mechanics and Mining Sciences*, vol. 112, pp. 95–107, 2018.

[23] C. S. Silveira, A. C. M. Alvim, and J. D. J. Rivero Oliva, "Radionuclide transport in fractured rock: numerical assessment for high level waste repository," *Science and Technology of Nuclear Installations*, vol. 2013, Article ID 827961, 17 pages, 2013.

[24] C. L. Zhang, J. Wang, and K. Su, "Concepts and tests for disposal of radioactive waste in deep geological formations," *Chinese Journal of Rock Mechanics and Engineering*, vol. 25, no. 4, p. 750, 2006.

[25] J. Wang, L. Chen, R. Su, and X. G. Zhao, "The Beishan underground research laboratory for geological disposal of high-level radioactive waste in China: planning, site selection, site

characterization and in situ tests," *Journal of Rock Mechanics and Geotechnical Engineering*, vol. 10, no. 3, pp. 411–435, 2018.

[26] X. G. Zhao, J. Wang, M. Cai et al., "In-situ stress measurements and regional stress field assessment of the Beishan area, China," *Engineering Geology*, vol. 163, pp. 26–40, 2013.

[27] Q. Y. Zhang, Q. Y. Ren, K. Duan et al., "Geo-mechanical model test on the collaborative bearing effect of rock-support system for deep tunnel in complicated rock strata," *Tunnelling and Underground Space Technology*, vol. 2019, Article ID 103001, 19 pages, 2019.

[28] Q. Y. Zhang, K. Duan, Y. Y. Jiao, and W. Xiang, "Physical model test and numerical simulation for the stability analysis of deep gas storage cavern group located in bedded rock salt formation," *International Journal of Rock Mechanics and Mining Sciences*, vol. 94, pp. 43–54, 2017.

[29] Q. Y. Zhang, X. T. Zhang, Z. C. Wang, W. Xiang, and J. H. Xue, "Failure mechanism and numerical simulation of zonal disintegration around a deep tunnel under high stress," *International Journal of Rock Mechanics and Mining Sciences*, vol. 93, pp. 344–355, 2017.

[30] H. P. Wang, Q. H. Zhang, L. Yuan, J. H. Xue, and B. Zhang, "Development of a similar material for methane-bearing coal and its application to outburst experiment," *Rock and Soil Mechanics*, vol. 36, no. 6, pp. 1676–1682, 2015.

[31] K. Wang, S. C. Li, Q. S. Zhang, X. Zhang, and C. Liu, "Development and application of new similar materials of surrounding rock for a fluid-solid coupling model test," *Rock and Soil Mechanics*, vol. 37, pp. 2521–2533, 2016.

[32] S. C. Li, X. D. Feng, S. C. Li, L. P. Li, and G. Y. Li, "Research and development of a new similar material for solid-fluid coupling and its application," *Chinese Journal of Rock Mechanics and Engineering*, vol. 29, no. 2, pp. 281–288, 2010.

[33] Q. Y. Zhang, S. C. Li, X. H. Guo, Y. Li, and H. P. Wang, *Cementitious Geotechnical Analogue Material For Iron Crystal Sand And Preparation Method*, Shandong University, Jinan, China, 2006.

[34] Q. Y. Zhang, S. C. Li, X. G. Chen et al., *Geomechanical Model Layer by Layer Compaction Air Drying Production and Grooving Burying Test Instrument Method*, Shandong University, Jinan, China, 2011.

[35] Q. Sheng, Z. Q. Yue, C. Lee, L. G. Tham, and H. Zhou, "Estimating the excavation disturbed zone in the permanent shiplock slopes of the Three Gorges Project, China," *International Journal of Rock Mechanics and Mining Sciences*, vol. 39, no. 2, pp. 165–184, 2002.

[36] P. Bossart, T. Trick, P. M. Meier, and J. C. Mayor, "Structural and hydrogeological characterisation of the excavation-disturbed zone in the opalinus clay (mont terri project, Switzerland)," *Applied Clay Science*, vol. 26, no. 1-4, pp. 429–448, 2004.

[37] C. C. Liu, X. K. Sun, X. F. Zhang, Q. Y. Zhang, Y. Chen, and J. X. Wang, "Physical model test on the deformation and fracturing process of underground research laboratory during excavation and overloading test," *Sustainability*, vol. 15, no. 12, p. 9416, 2023.

[38] S. W. Chen, C. H. Yang, G. B. Wang, E. B. Li, and L. Chen, "Experimental study of acoustic emission monitoring in situ excavation damage zone of Beishan exploration tunnel," *Rock and Soil Mechanics*, vol. 2, no. 38, pp. 349–358, 2017.

[39] E. B. Li, Y. Han, Y. H. Tan et al., "Field measuring test on internal displacement of surrounding rock during whole excavation process of Beishan exploration tunnel," *Chinese Journal of Rock Mechanics and Engineering*, vol. 11, pp. 2741–2754, 2017.

[40] C. C. Liu, Q. Y. Zhang, K. Duan, W. Xiang, and Y. Y. Jiao, "Development and application of an intelligent test system for the model test on deep underground rock caverns," *Energies*, vol. 13, no. 2, p. 358, 2020.

[41] Q. Y. Zhang, C. C. Liu, K. Duan, Z. J. Zhang, and W. Xiang, "True Three-dimensional geomechanical model tests for stability analysis of surrounding rock during the excavation of a deep underground laboratory," *Rock Mechanics and Rock Engineering*, vol. 53, no. 2, pp. 517–537, 2020.

[42] Q. Y. Zhang, Y. Zhang, K. Duan, C. C. Liu, Y. S. Miao, and D. Wu, "Largescale geo-mechanical model tests for the stability assessment of deep underground complex under true-triaxial stress," *Tunnelling and Underground Space Technology*, vol. 83, pp. 577–591, 2019.